Effects of Bandwidth on Observable Multipath Clustering in Outdoor/Indoor Environments for Broadband and Ultrawideband Wireless Systems

Wei-Ju Chang and Jenn-Hwan Tarng, *Senior Member, IEEE*

***Abstract*—A multipath-clustering phenomenon, which is caused by the fact that scatterers tend to group together in realistic environments, has a significant impact on the channel capacity. For a band-limited system, due to the limitation of the signal time resolution, observable multipath-clustering is affected not only by propagation environments but also by the signal bandwidth. Since a larger bandwidth gives better time resolution, it is possible to observe more multipath components and, therefore, stronger clustering effects. In this paper, a new method based on the $\Delta-K$ model for multipath times of arrival (TOAs) is proposed to investigate and quantify the effect of signal bandwidth on observable multipath clustering. Furthermore, to completely characterize the time dispersion characteristics of the channel, a statistical model using a power ratio, a decay constant, and the Rician factor to describe multipath averaged power decay and amplitude fading is proposed. Newly derived formulas are given to relate the model parameters of a wideband signal, including those of the multipath TOA, averaged power decay, and amplitude fading, to those of a narrowband signal. The channel parameter estimation methods have been extensively validated by comparing the computed channel parameters with the ones extracted from the measured channel responses of 1.95 and 2.44 GHz broadband radios in metropolitan and suburban areas, and of 3–5 GHz ultrawideband signals in indoors.**

***Index Terms*—Channel impulse response, multipath clustering, radio propagation, ultrawideband (UWB), $\Delta-K$ model.**

I. Introduction

RECENTLY, systems beyond 3G (B3G) have been actively discussed in various forums and organizations. According to the International Telecommunication Union Radiocommunication Sector preliminary recommendation [1], for B3G systems, new radio access technologies using a wider bandwidth than that of the current wireless communication system are required to support higher rate data transmissions. For instance, the ultrawideband (UWB) radio technology has been considered as one of the viable candidates for B3G systems due to its potential strength to provide a high channel capacity with an extremely wide transmission bandwidth [2]. According to the Federal Communications Commission (FCC) regulations of UWB radio technology and systems [3], a minimum bandwidth limitation of a UWB radio signal is 500 MHz, and the frequency band from 3.1 to 10.6 GHz is allowed for indoor communication applications.

In order to realize the B3G systems, a thorough understanding of the time dispersion characteristics of radio multipath propagation channels is required. In high-speed wireless data transmission, severe frequency-selective fading of a multipath channel causes intersymbol interference and leads to a significant problem for the systems. To solve the problem, modeling of a multipath time of arrival (TOA) that is particular on the multipath-clustering phenomenon is a fundamental and important work. The phenomenon according to channel measurements [4], [5] showed multipath arrivals in a cluster rather than in a continuum, as is customary for narrowband channels. This is because the scatterers are resolved in groups by the system with fine or very fine time resolution. Modeling of this phenomenon helps the design of an equalizer or Rake receiver, such as the design of equalizers with unequal tap spacing or the design of a selective Rake receiver and partial Rake receivers [6]. In addition, in [7], it is shown that unclustered models tend to overestimate the channel capacity as compared with the case that multipath components (MPCs) are, indeed, clustered. This phenomenon was found in indoor and outdoor broadband radio channels [4]–[6], [8], as well as in indoor UWB channels [9]–[11].

For statistical models, the Saleh–Valenzuela (S–V) [4] and $\Delta-K$ models [8] are two well-recognized models to characterize the multipath-clustering phenomenon. In the S–V model, two Poisson models are applied to characterize this phenomenon. The first Poisson model describes the cluster arrival time, and the second Poisson model describes the arrival times of MPCs within each cluster. In the $\Delta-K$ model, the multipath-clustering phenomenon is characterized by a modified Poisson process, which models the path occurrence probability as a function of whether or not a path arrival is in the previous bin. It is noted that the $\Delta-K$ model has shown a good fit to the empirical data that were collected in several urban [8] and indoor environments [5], [12], [13] and has been used for UWB indoor channel modeling [14], [15].

Manuscript received February 29, 2004; revised February 4, 2005, July 12, 2005, December 28, 2005, March 26, 2006, July 18, 2006, and September 10, 2006. This work was supported by the National Science Council of the Republic of China under Contracts NSC-93-2752-E-002-009-PAE, NSC 93-2752-E-009-003-PAE, and NSC 94-2213-E-009-070. The review of this paper was coordinated by Prof. A. Abdi.

W.-J. Chang is with the Department of Communication Engineering, National Chiao Tung University, Hsinchu 300, Taiwan, R.O.C., and also with Chunghwa Telecom Laboratories, Taoyuan 326, Taiwan, R.O.C. (e-mail: wjcha@cht.com.tw).

J.-H. Tarng is with the Department of Communication Engineering, National Chiao Tung University, Hsinchu 300, Taiwan, R.O.C. (e-mail: j4t@mail.nctu.edu.tw).

Color versions of one or more of the figures in this paper are available online at http://ieeexplore.ieee.org.

Digital Object Identifier 10.1109/TVT.2007.897658

Although there are many researches who are focusing on the exploration or modeling of the multipath-clustering phenomenon, few researches are focused on the effect of signal bandwidth on observed multipath clustering so far. It is easily understood that in the observation of multipath clustering of a radio channel using a band-limited signal, the result is mainly affected by the signal resolution, which is the reciprocal of the signal bandwidth. In this paper, based on the $\Delta-K$ model, new formulas are derived to describe the relationships between the observed TOA model parameters of narrowband signals and those of wideband signals. Through this approach, the effect of signal bandwidth on the observable multipath clustering is explored. Furthermore, to completely characterize the time dispersion characteristics of the channel, a model using a power ratio, a decay constant, and the Rician factor to describe multipath averaged power delay profile (aPDP) and amplitude fading is proposed. Formulas to relate these model parameters of a wideband signal to those of a narrowband signal are also derived. Here, the model parameter estimation methods have been extensively validated by comparing the computed channel parameters with the ones extracted from the measured channel responses of 1.95 and 2.44 GHz broadband radios in metropolitan and suburban areas and of 3–5 GHz UWB signals in indoors.

II. Effect of Bandwidth on Observable Multipath Clustering

A. $\Delta-K$ Model

The $\Delta-K$ model is initiated by Turin *et al.* [16], [17] and developed by Suzuki [8] to describe the TOAs of MPCs by taking multipath clustering into account. In the model, the axis of excess delay times (relative to the propagation delay of the direct path between transmitting and receiving antennas) is partitioned into bins with width Δ [8]. The probability of having a path in bin i is a function of whether or not an arrival occurred in the previous bin and is a function of the empirical probability of path occurrences at different delays, which is based on measurements. It can be stated as the branching process of Fig. 1: The probability of having a path in bin i is equal to λ_i if there is no path in the $(i-1)$th bin; otherwise, it is increased by a factor K due to a multipath-clustering effect. Note that both the path occurrence probabilities, λ_i and $K \cdot \lambda_i$, are equal to or less than 1. When $K > 1$, the process exhibits a clustering property and large K represents a large clustering effect. For $K = 1$, this process reverts to a standard Poisson process.

It is noted that this model is applicable upon replacing K by k_i, which is a function of the bin number i [8], [12], [18]. From the branching process shown in Fig. 1 by replacing K by k_i, it is found that P_i, which is the probability of having a path in bin i, is equal to the sum of the probabilities $(1 - P_{i-1}) \cdot \lambda_i$ and $P_{i-1} \cdot k_i \cdot \lambda_i$. After some derivations, λ_i is given as

$$\lambda_i = \frac{P_i}{(k_i - 1) \cdot P_{i-1} + 1}, \qquad i \geq 2 \tag{1}$$

where $\lambda_1 = P_1$.

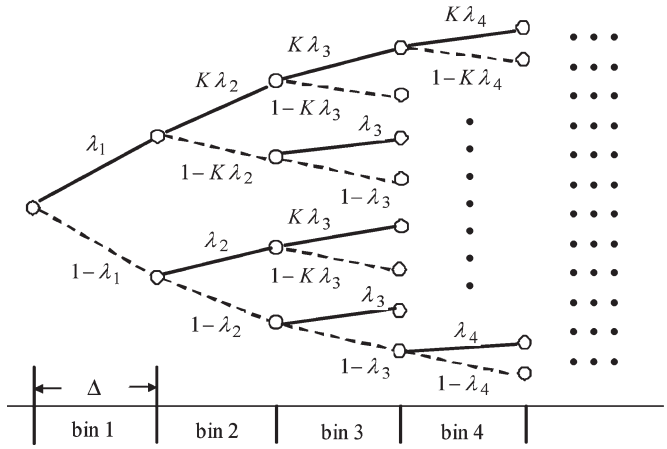

Fig. 1. $\Delta-K$ process.

It is noted that Δ is a model parameter to be chosen [8], [16]. However, according to the assumption in these papers that each bin contains either one path or no path, it is reasonable to set Δ as the signal time resolution, which is a reciprocal of the signal bandwidth, of the specific radio system [5], [13], [18]. This is because two or more paths arriving within the same time resolution interval cannot be resolved as distinct paths for a band-limited radio system [5]. Based on this fact, it is expected that systems with different bandwidths may observe different multipath-clustering phenomena and yield different channel model parameters for a specific environment because of the fact that the number of resolvable MPCs and clusters is changed with signal time resolution.

B. Effect of Bandwidth on Observable Multipath Clustering

To explore bandwidth dependency of the model parameters, which include the clustering parameter, formulas to describe the relationships between observed model parameters of narrowband signals and those of wideband signals are derived. It is noted that the bandwidth of the wideband signal is confined to be n times of the narrowband signal's, where n is a positive integer. For convenience, the parameters with a subscript f or F correspond to those of bandwidth f or F, respectively, where $F = n \cdot f$.

1) Formulas for Wideband to Narrowband: Since a bin width is inversely proportional to its signal bandwidth, Δ_f is equal to $n \cdot \Delta_F$, where Δ_f and Δ_F are the bin widths of the systems with signal bandwidths f and F, respectively. Therefore, when a received path occurs at bin i of a signal with bandwidth f, the path should arrive at one or more of the bins covering from the $(n \cdot i - n + 1)$th bin to the $(n \cdot i)$th bin for the signal with bandwidth F, which is due to the increase of the time resolution interval.

With the above analysis, $\lambda_{i,f}$ and $P_{i,f}$ are derived in terms of $\lambda_{j,F}$ and $P_{j,F}$ by (2) and (3), respectively. That is,

$$\lambda_{i,f} = 1 - \prod_{r=1}^{n} (1 - \lambda_{A+r,F}) \tag{2}$$

where $A = n \cdot i - n$. $P_{i,f}$, in (3), is shown at the bottom of the next page.

Substituting $\lambda_{i,f}$ and $P_{i,f}$ into (1), $k_{i,f}$ is obtained. Here, let $n = 2$, the analytical relationship between $k_{i,f}$ and $k_{2\cdot i-1,F}$ is found and written as

$$(k_{i,f}-1)=(k_{2\cdot i-1,F}-1)\cdot\frac{\lambda_{2\cdot i-1,F}(1-\lambda_{2\cdot i,F})}{[\lambda_{2\cdot i,F}+\lambda_{2\cdot i-1,F}(1-\lambda_{2\cdot i,F})]}\cdot\frac{[k_{2\cdot i-2,F}\cdot\lambda_{2\cdot i-2,F}\cdot P_{2\cdot i-3,F}+\lambda_{2\cdot i-2,F}(1-P_{2\cdot i-3,F})]}{[P_{2\cdot i-3,F}+\lambda_{2\cdot i-2,F}(1-P_{2\cdot i-3,F})]}. \quad (4)$$

On the right-hand side of (4), magnitudes of the second and third factors are in the range of 0–1. From (4), it is found that $k_{i,f}$ is smaller than $k_{2\cdot i-1,F}$ if $k_{2\cdot i-1,F} > 1$. It means that a wider bandwidth signal observes a stronger multipath-clustering phenomenon. It is noted that $k_{2\cdot i-1,F} \cong k_{2\cdot i,F}$, which is found from measurement data and is shown in Section V.

2) Formulas for Narrowband to Wideband: With (2) and (3), the observed model parameters of a narrowband signal cannot determine those of a wideband signal due to the limited conditions. For $n = 2$, one extra condition is needed to determine three unknown parameters $\lambda_{2\cdot i-1,F}$, $\lambda_{2\cdot i,F}$, and $P_{2\cdot i-1,F}$ with those of bandwidth f, $\lambda_{i,f}$, and $P_{i,f}$. Here, the condition is given by assuming $\lambda_{2\cdot i-1,F} = \lambda_{2\cdot i,F}$, i.e., the path arrival rates of two neighboring bins are equal. It is because for both outdoor broadband and indoor UWB radio channels, the multipath excess delay time is much larger than the time resolution (bin width). Based on this assumption, $\lambda_{2\cdot i-1,F}$ and $\lambda_{2\cdot i,F}$ are solved from (2), i.e.,

$$\lambda_{2\cdot i-1,F} = \lambda_{2\cdot i,F} = 1 - \sqrt{1-\lambda_{i,f}}. \quad (5)$$

However, our assumption may lead to underestimate $\lambda_{2\cdot i-1,F}$ and overestimate $\lambda_{2\cdot i,F}$ since the path arrival rate decreased asymptotically with bin number. To reduce the estimation errors, $\lambda_{2\cdot i-1,F}$ and $\lambda_{2\cdot i,F}$ from (5) are modified using the interpolation method and are given by (6a) and (6b), respectively, as follows:

$$\lambda_{2\cdot i-1,F}=\min\left\{1,\left[\lambda_{2\cdot i-1,F}+\frac{1}{4}\cdot(\lambda_{2\cdot i-1,F}-\lambda_{2\cdot i+1,F})\right]\right\} \quad (6a)$$

$$\lambda_{2\cdot i,F}=\lambda_{2\cdot i-1,F}-\frac{1}{4}\cdot(\lambda_{2\cdot i-1,F}-\lambda_{2\cdot i+1,F}). \quad (6b)$$

It is noted that $\lambda_{2\cdot i-1,F}$ and $\lambda_{2\cdot i+1,F}$ on the right-hand side of (6a) and (6b) are calculated from (5). Then, from (3), with $n = 2$, $P_{2\cdot i-1,F}$ is solved and given by (7a) as follows:

$$P_{2\cdot i-1,F} = (P_{i,f} - \lambda_{2\cdot i,F})/(1-\lambda_{2\cdot i,F}). \quad (7a)$$

Here, $P_{2\cdot i,F}$ is computed by averaging its neighboring points and is given by (7b) as follows:

$$P_{2\cdot i,F} = (P_{2\cdot i-1,F} + P_{2\cdot i+1,F})/2. \quad (7b)$$

Substituting $\lambda_{j,F}$ and $P_{j,F}$ into (1), $k_{j,F}$ is obtained. Through the above approaches, the model parameters of a wideband signal $\lambda_{j,F}$, $P_{j,F}$, and $k_{j,F}$ are determined by those of a narrowband signal $\lambda_{i,f}$ and $P_{i,f}$, for $n = 2$. Furthermore, by repeating the procedures, this method can be extended to $n = 2^m$, where $m = 2, 3, \ldots$.

III. Effect of Bandwidth on Multipath Averaged Power Decay and Amplitude Fading

To completely characterize the time dispersion characteristics of the channel, effects of bandwidth on multipath averaged power decay and amplitude fading are analyzed as follows.

A. Statistical Model for Multipath Averaged Power Decay and Amplitude Fading

In many literatures for broadband and UWB radio channel modeling [15], [19], the small-scale aPDP $\overline{g}(\tau)$ is modeled by an exponential time decay function with a stronger first bin and is expressed as

$$\overline{g}(\tau) = \overline{G}_1\left[\delta(\tau_1) + \sum_{i=2}^{L}\gamma\,\exp\left[-(\tau_i-\tau_2)/\Gamma\right]\delta(\tau_i)\right] \quad (8)$$

where $\overline{G}_1$ is the mean power of the first bin, τ_i is the relative time delay of bin i and is equal to $(i-1)\cdot\Delta$, γ is the power ratio that is defined as the ratio of the second bin's mean power to the first bin's mean power, Γ is the exponentially power decay constant, and δ is the Dirac delta function. From our extended measurement data at indoor environments, one of the examples shown in Fig. 2, it is found that this model well describes the measured aPDP.

Based on our measurement data, it is found that the amplitude fading of the first bin follows a Rician distribution with a large Rician factor, and the later bins tend to follow the Rayleigh statistics (the Rician factor is closed to zero), as shown in Fig. 3. It is noted that measured points 1–12 are in line-of-sight (LOS) situations and the rest of the points are in non-LOS (NLOS) situations. Details of measurements are described in Section IV-B.

B. Effect of Bandwidth on Multipath Averaged Power Decay and Amplitude Fading

1) Formulas for Wideband to Narrowband: For an uncorrelated scattered radio propagation channel [20], bins' amplitudes

$$P_{i,f} = \begin{cases} P_{A+1,F} + (1-P_{A+1,F})\lambda_{A+2,F}, & n = 2 \\ P_{A+1,F} + (1-P_{A+1,F})\left\{\lambda_{A+2,F} + \sum_{r=3}^{n}\left[\lambda_{A+r,F}\prod_{s=3}^{r}(1-\lambda_{A+s-1,F})\right]\right\}, & n \geq 3 \end{cases} \quad (3)$$

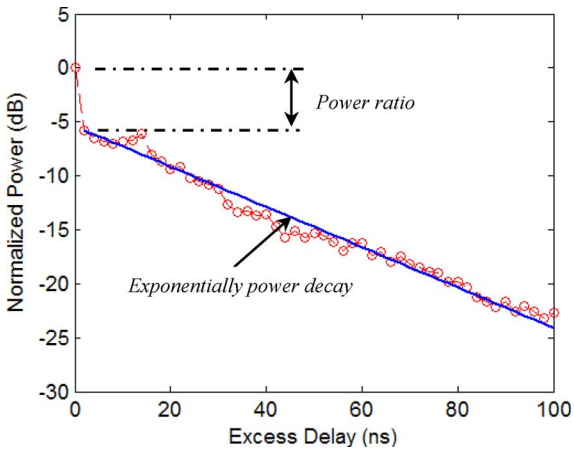

Fig. 2. Averaged power delay profile of a 500-MHz-bandwidth UWB signal at an indoor environment and under the NLOS condition. The wavy line shows the measured profile. The straight line, which is obtained by a best fit procedure, represents an exponential decay line.

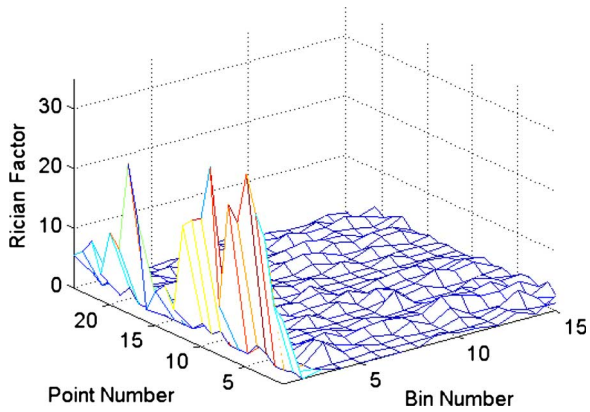

Fig. 3. Rician factors of the first 15 bins of each measured point at indoor environments with 2 GHz bandwidth are shown. The total number of measured points is 24. It is found that most LOS situations and NLOS situations having strong direct penetration path have larger Rician factors of the first bin to compare with other situations.

are distributed independent of one another, and the averaged bin power is calculated by the power sum of multipath in a bin. For example, the averaged power sum of two successive bins for bandwidth F is equal to the averaged power of the corresponding bin for bandwidth f when $n = 2$, i.e., $\overline{G}_{i,f} = \overline{G}_{2\cdot i-1,F} + \overline{G}_{2\cdot i,F}$. From (8) and $n = 2$, $\overline{G}_{i,f}$ is expressed by

$$\begin{cases} \overline{G}_{1,f} = 1+\gamma_F \\ \overline{G}_{i,f} = \gamma_F \cdot [\exp(-\Delta_F/\Gamma_F)+\exp(-2\cdot\Delta_F/\Gamma_F)] \\ \qquad \cdot \exp\left[-(i-2)\cdot\Delta_f/\Gamma_F\right], \qquad i \geq 2 \end{cases} . \tag{9}$$

From (9), it is found that $\overline{G}_{i,f}$ is exponentially decayed from bin 2 with a time decay constant Γ_F. It represents that the decay constant is independent of signal bandwidth, i.e., $\Gamma_f = \Gamma_F$.

From (9), the power ratio $\gamma_f = \overline{G}_{2,f}/\overline{G}_{1,f}$ is expressed by

$$\gamma_f = \frac{\gamma_F}{1+\gamma_F} \cdot [\exp(-\Delta_F/\Gamma_F) + \exp(-2\cdot\Delta_F/\Gamma_F)]. \tag{10}$$

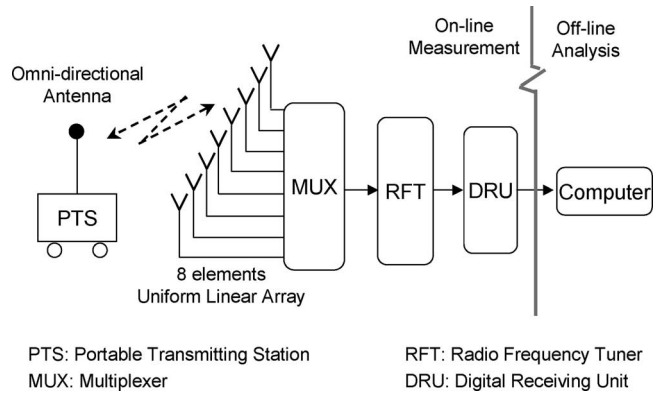

Fig. 4. System diagram of the RUSK wideband vector channel sounder.

From (10), γ_f is greater than γ_F if $\Gamma_F \gg \Delta_F$, which is true for the most indoor UWB channels that their decay constants are larger than 10 ns and their bin widths are smaller than 2 ns.

The Rician statistics is mainly characterized by a Rician factor R, which is defined as the power ratio of the specular/LOS path to the scattered multipath. For the first bin, when the signal bandwidth changes from F to f, the specular/LOS path power is unchanged, but the scattered multipath power is increased by $\overline{G}_{2,F}$ due to the increase of the bin width and no specular/LOS path in bin 2 (its Rician factor is closed to 0). Therefore, R_f, after simple derivations, is given by

$$R_f = \frac{R_F}{1+(R_F+1)\cdot\gamma_F}. \tag{11}$$

Since the denominator of (11) is always larger than one, R_f is smaller than R_F. The reason for this result is that the total number of scattered multipath in the first bin is increased when the signal bandwidth is decreased, which yields an increase of the scattered power. It is noted that (11) is not so meaningful for the latter bins since their amplitude fading follow a Rayleigh distribution with their Rician factors all close zero.

2) Formulas for Narrowband to Wideband: With (10) and the condition $\Gamma_f = \Gamma_F$, it is easily found that γ_F is given by

$$\gamma_F = \frac{\gamma_f}{[\exp(-0.5\cdot\Delta_f/\Gamma_f)+\exp(-\Delta_f/\Gamma_f)]-\gamma_f}. \tag{12}$$

Substituting (12) into (11), R_F is expressed by

$$R_F = R_f \cdot \frac{1+\frac{\gamma_f}{[\exp(-0.5\cdot\Delta_f/\Gamma_f)+\exp(-\Delta_f/\Gamma_f)]-\gamma_f}}{1-R_f\cdot\frac{\gamma_f}{[\exp(-0.5\cdot\Delta_f/\Gamma_f)+\exp(-\Delta_f/\Gamma_f)]-\gamma_f}}. \tag{13}$$

IV. Measurement Setup and Environment

A. Broadband Outdoor Channels

For outdoor environments, the RUSK broadband vector channel sounder [21] is employed to measure the band-limited channel impulse response. The system diagram of the channel sounder is illustrated in Fig. 4. It consists of a mobile transmitter with an omnidirectional antenna and a fixed receiver with an eight-element uniform linear array antenna. A maximum

TABLE I
MEASUREMENT SETUP AND ENVIRONMENTS FOR THE BROADBAND OUTDOOR CHANNEL MEASUREMENTS

Site No.	Urban 1	Urban 2	Suburban
Measurement Environment	Heavily built up area with an average building height of 10 stories. The maximum one is 26 stories.	Heavily built up area with an average building height of 10 stories. The maximum one is 20 stories.	Small village with buildings of 3~6 stories and gardens with trees and pools.
Numbers of sampled routes and points	Total number of the sampled routes is 7 and each route has 150 meters long approximately. Total sampled points are about 600. Most of them are in NLOS situation.	Total number of the sampled routes is 8 and each route has 250 meters long approximately. Total sampled points are about 900. Most of them are in NLOS situation.	Total number of the sampled routes is 5 and each route has 150 meters long approximately. Total sampled points are about 400. Most of them are in NLOS situation.
Center Frequency	2.44 GHz	1.95 GHz	1.95 GHz
Bandwidth	120 MHz	50 MHz	50 MHz
Receiver	On the rooftop of a 11-floor building.	On the rooftop of a 12-floor building.	On the rooftop of a 8-floor building.

120-MHz broadband radio signal can be generated by periodic multifrequency signal excitation. It is very helpful for this study, because radio channel data for the narrowband signal can be intercepted from the measurement data of the wideband signal.

Measurements of broadband radio channel impulse response were performed at three outdoor sites in Taipei (a large city) and a suburban area. A summary of the measurement setup and environments for these sites is given in Table I. At each site, the fixed receiver and its antenna were mounted on a rooftop; the mobile transmitter and its antenna were carried by a car with an antenna height of 1.8 m above the ground. Measurement was done along selected routes with a speed of 10 km/h approximately, and the channel responses were sampled in a time grid of 1000.448 ms. It is noted that the distance between two neighboring channel response sampling points are around 10–20 times of the wavelength of the center frequency, which means that the small-scale measurements were not performed at outdoor sites.

B. UWB Indoor Channels

A schematic diagram of the UWB indoor channel measurement system is shown in Fig. 5. An Agilent 8719ET vector network analyzer (VNA) was used for measuring the frequency response of the channel. The transmitted signal is sent from the VNA to the transmitting antenna through a low-loss 10-m coaxial cable. Both the transmitting and receiving antennas (EM-6865) are vertical-polarized and omnidirectional in the H-plane. They are biconical antennas covering 2–18 GHz. The signal from the receiving antenna is returned to the VNA via a low-loss 30-m coaxial cable and is amplified by a low-noise amplifier (LNA) with a gain of 30 dB connecting to the VNA. The VNA records the variation of 801 complex tones across the 3–5-GHz frequency range by measuring the S-parameter

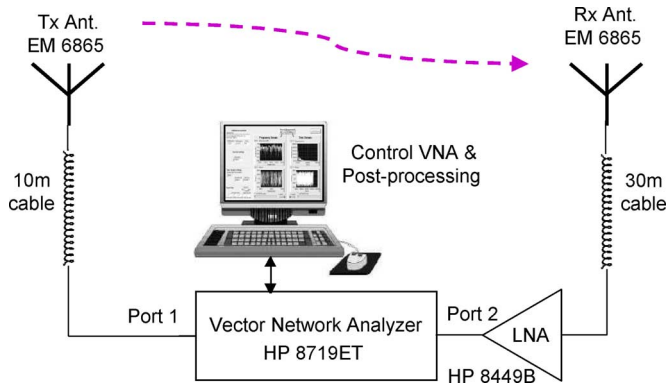

Fig. 5. Schematic diagram of the UWB indoor channel measurement system.

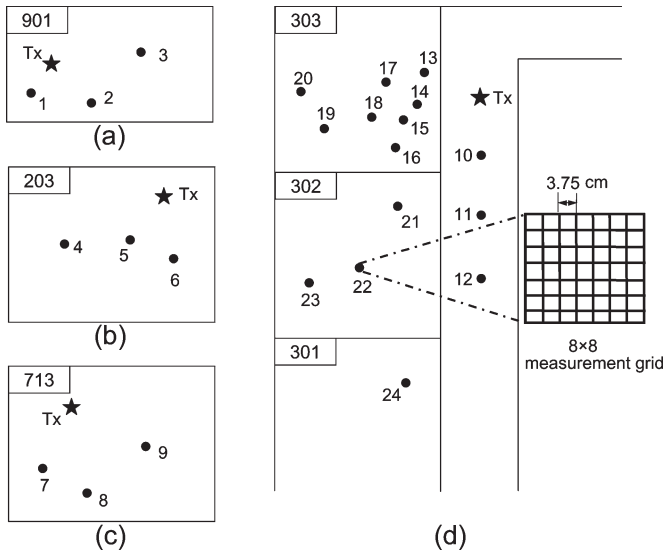

Fig. 6. Layouts of four sites where the UWB indoor channel measurements were performed. (a) Laboratory 901. (b) Classroom 203. (c) Computer room 713. (d) Classrooms 301–303 and corridors. Locations of the transmitter (Tx) and the receiver are shown by "△" and "•," respectively.

S_{21} of the UWB channel, which is essentially the transfer function of the channel. The time-domain channel response can be obtained by taking the inverse Fourier transform of the frequency-domain channel response.

UWB propagation experiments were performed in three different floors of Engineering Building Number Four at the National Chiao-Tung University, Hsinchu, Taiwan, R.O.C. Fig. 6(a)–(d) shows the floor layouts of the measurement sites, including a laboratory, a classroom, a computer room, and corridors/classrooms, respectively. Room 901 is a laboratory with some equipment and iron tables. The classroom has many wooden chairs, and the computer room has ten iron tables and 50 computers. At these sites, all measured points are under the LOS condition. At the last site, the transmitter (Tx) is located at the corridor, and 15 measured points are carefully planned to include LOS and NLOS propagations. At each measured point, 64 channel frequency responses were sampled at 64 subpoints, which are arranged in an 8×8 square grid, as shown in Fig. 6(d). The spacing between two neighboring subpoints is 3.75 cm, which is equal to half the wavelength of the center frequency. In each measurement, both the

transmitting and receiving antennas are fixed with the same height of 1.6 m.

Here, these 24 measured points are classified into two scenarios, the "Indoor LOS" and the "Indoor NLOS." The "Indoor LOS" represents all the measurements in the LOS condition, which contains measured points 1–12. The distance between the transmitter and each receiver is ranged from 2 to 9 m. The "Indoor NLOS" represents all the measurements in the NLOS condition, which contains measured points 13–24. The distance between the transmitter and each receiver is ranged from 3 to 18 m.

V. Validations and Discussions

In this paper, the $\Delta-K$ model parameters are extracted from the measured instantaneous power delay profiles (iPDPs) for both outdoor and indoor measurement sites. However, the model parameters of aPDP and amplitude fading are only computed and validated for indoor sites since the small-scale measurements were not performed at outdoor sites.

A. Data Analysis and Processing

1) Measurement Data Processing: Before performing the $\Delta-K$ model parameters extraction, the measured iPDPs were processed according to the following procedures. It is noted that a propagation path may be undetected in an iPDP due to the amplitude fading. Therefore, to increase the reliability of the estimation, only the iPDPs with a large signal-to-noise ratio (SNR) are considered for extracting the $\Delta-K$ model parameters.

a) Delay translation: Since the absolute propagation delays of the received signals vary from one location to another, an appropriate delay reference is needed to characterize the relative delays of each path. Here, the measured delay time of each iPDP is shifted by the propagation delay, which is equal to d/c, where d is the T–R separation distance, and c is the speed of light.

b) iPDP selection: Since the path detection algorithm that is shown in the following is in connection with the noise floor, most of the long-delay paths cannot be detected for a measured iPDP with a low SNR. Here, only the measured iPDPs with a high SNR (highest peak $>$ noise floor $+$ 20 dB) were selected to extract the model parameters. Therefore, the effect of amplitude fading on the model parameters, which is not considered in our approach, is reduced, especially for the bins with short delays because of their high powers.

c) Path detection: To detect the presence of a path in any bin, we adopt the approach presented in [5], [13], and [22] by choosing an α-dB threshold relative to the highest peak power in the iPDP. In addition to that, the path power must also exceed 6 dB above the noise floor [19] to reduce the influence of noise on path detection. The noise floor for each iPDP is obtained by computing the average power from the portion of the iPDP that is measured before the first MPC arrives. To choose a reasonable value of α, the effects of this value on some channel statistics such as the average mean excess delay, average rms delay spread, standard deviation of rms delay spread, and average number of paths were analyzed. It is found that the average mean excess delay, average rms delay spread, and standard deviation of rms delay spread are all in the saturation region when the threshold value is larger than around 20 dB for all measurement sites. However, a different phenomenon is found for an average number of paths, which is increased as the threshold value. It is simply because a larger threshold value will capture a larger number of paths. However, this increase does not influence the value of the model parameters because these paths have very low power. For example, when α is larger than around 20 dB, P_i, λ_i, and k_i with small i will not be changed with α. Therefore, the relative power threshold value was chosen as 20 dB in this paper.

For the computation of model parameters, the path arrivals of an iPDP is described by a path indicator sequence of "0"s and "1"s, where a "1" indicates the presence of a path in a given bin, and a "0" represents the absence of a path in that bin.

Furthermore, for the aPDP and small-scale amplitude fading model parameters extraction, the aPDP of each measured point at indoor sites is computed by averaging the iPDPs sampled at the 64 subpoints.

2) Model Parameter Extraction: Here, we follow the method proposed in [13] for $\Delta-K$ model parameters extraction. Compared to the model parameter extracting method used in previous works [5], [8], [12], the method directly describes the bin-by-bin conditional path arrival probabilities and provides an easier mean to calculate λ_i and k_i.

In the method, all the selected path indicator sequences of each measurement site were collected to compute the $\Delta-K$ model parameters through the following procedures.

a) P_i computation:

$$P_i = \frac{N_{1,i}}{N_{\text{total}}} \tag{14}$$

where $N_{1,i}$ is the number of points that the path indicator is 1 at bin i, and N_{total} is the number of total selected points for this site. It is noted that the average number of paths $(\text{NP}_{\alpha\,\text{dB}})$, which is one of the key channel characteristics for broadband and UWB radio propagations, can be calculated as the sum of P_i, i.e., $\text{NP}_{\alpha\,\text{dB}} = \sum_i P_i$. In this paper, α is chosen to be 20.

b) λ_i computation:

$$\lambda_i = \frac{N_{01,i}}{N_{00,i} + N_{01,i}} \tag{15}$$

where $N_{01,i}$ is the number of points that the path indicator is 0 at the $(i-1)$th bin and is 1 at the ith bin, and $N_{00,i}$ is the number of points that the path indicator is 0 at both the $(i-1)$th and the ith bins.

c) k_i computation:

$$k_i = \frac{N_{11,i}}{\lambda_i \cdot (N_{10,i} + N_{11,i})} \tag{16}$$

where $N_{11,i}$ is the number of points that the path indicator is 1 at both the $(i-1)$th and the ith bins, and $N_{10,i}$ is the number of points that the path indicator is 1 at the $(i-1)$th bin and is 0 at the ith bin.

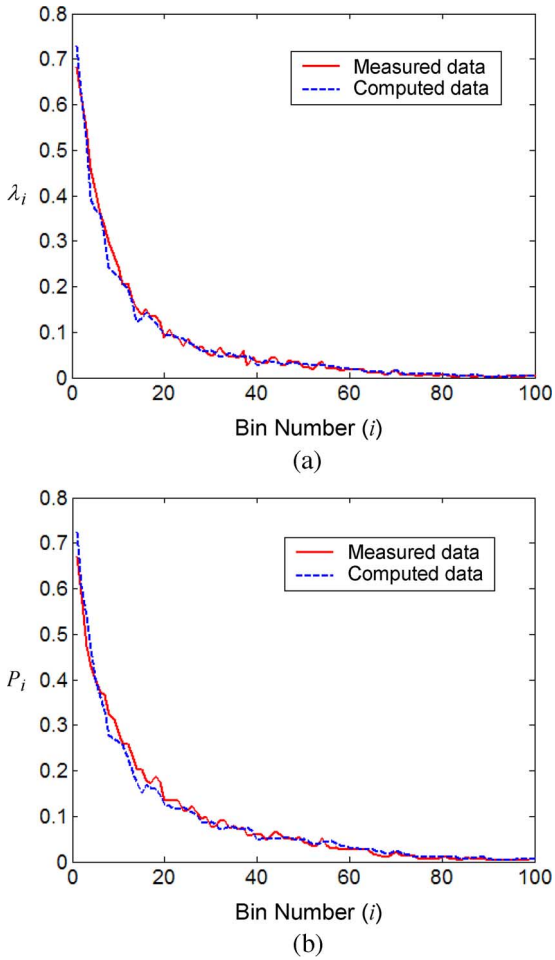

Fig. 7. Comparisons of the measured and computed results of (a) the path arrival rate λ_i and (b) the path occurrence probability P_i of the "Urban 1" site with 60 MHz bandwidth for $n = 2$.

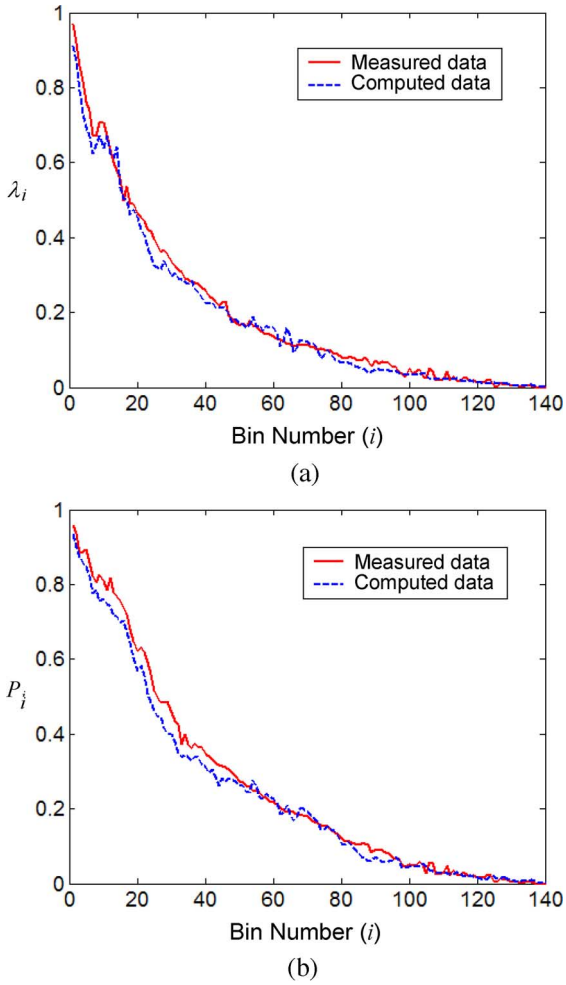

Fig. 8. Comparisons of the measured and computed results of (a) the path arrival rate λ_i and (b) the path occurrence probability P_i of the "Indoor NLOS" site with 1 GHz bandwidth for $n = 2$.

Furthermore, the model parameters of averaged power decay γ and Γ are extracted from the aPDP by the best fit procedure for each measured point at indoor sites. Finally, the Rician factor is obtained by fitting the cumulative distribution function of the 64 subpoints' amplitude to that of a Rician distribution for each measured point at indoor sites.

B. Validations

Fig. 7(a) and (b) illustrates the measured and computed λ_i and P_i of a 60-MHz-bandwidth signal at the "Urban 1" site, respectively. In these figures, the discrete points of λ_i or P_i are connected by curves for clarity. The computed λ_i and P_i are achieved from the measured λ_j and P_j of a 30-MHz-bandwidth signal by using (6) and (7), respectively. The comparison shows that the proposed method yields a good prediction accuracy of λ_i, with $m_{e-\lambda} = -0.0632$ and $\sigma_{e-\lambda} = 0.0906$, and P_i, with $m_{e-P} = -0.0669$ and $\sigma_{e-P} = 0.0922$. Here, $m_{e-\lambda}$ and m_{e-P} represent the mean of the relative error (i.e., the ratio of the difference between the computed and the measured data to the measured data) of λ_i and P_i, respectively. $\sigma_{e-\lambda}$ and σ_{e-P} are the standard deviations of the relative error of λ_i and P_i, respectively. For UWB radio propagation in indoor environments, Fig. 8(a) and (b) illustrates the measured and computed λ_i and P_i, respectively, of a 1-GHz-bandwidth signal at the "Indoor NLOS" site. Here, the computed data for the 1-GHz-bandwidth signal is achieved from the measured data of a signal with 500 MHz bandwidth using (6) and (7). For conciseness, the results of other sites are not illustrated. In Table II, the values of $m_{e-\lambda}$, $\sigma_{e-\lambda}$, m_{e-P}, and σ_{e-P} for $n = 2$ at all sites are listed. From Table II, it is found that the absolute value of $m_{e-\lambda}$ and m_{e-P} are both less than 0.1, which validates our proposed method. The small difference between the measured and the computed parameter values may be mainly due to the amplitude fading, which is dependent on the bandwidth and is not considered in our approach. In addition to that, the small fluctuations of λ_i and P_i, as shown in Figs. 7 and 8, also lead to some prediction errors because it is inconsistent with our assumption that λ_i and P_i decrease asymptotically with bin number.

For the case of $n = 4$, Fig. 9(a) and (b) illustrates the measured and computed λ_i and P_i of a 120-MHz-bandwidth signal at the "Urban 1" site, respectively. Here, the computed data for the 120-MHz-bandwidth signal is achieved from the measured data of a signal with 30 MHz bandwidth. The comparison shows that our proposed method also yields a good prediction accuracy of λ_i and P_i for $n = 4$. The $m_{e-\lambda}$, $\sigma_{e-\lambda}$, m_{e-P}, and σ_{e-P} for $n = 4$ at all sites are calculated and listed in Table III.

TABLE II
VALUES OF $m_{e-\lambda}, \sigma_{e-\lambda}, m_{e-P}$, AND σ_{e-P} FOR $n = 2$

Measurement Sites	Bandwidth (F)	$m_{e\text{-}\lambda}$	$\sigma_{e\text{-}\lambda}$	$m_{e\text{-}P}$	$\sigma_{e\text{-}P}$
Urban 1	120 MHz	-0.0853	0.0902	-0.0790	0.0931
Urban 2	50 MHz	-0.0793	0.0928	-0.0763	0.0911
Suburban	50 MHz	-0.0924	0.1087	-0.0891	0.1012
Indoor LOS	2 GHz	-0.0911	0.1070	-0.0886	0.1031
Indoor NLOS	2 GHz	-0.0786	0.1125	-0.0807	0.1007

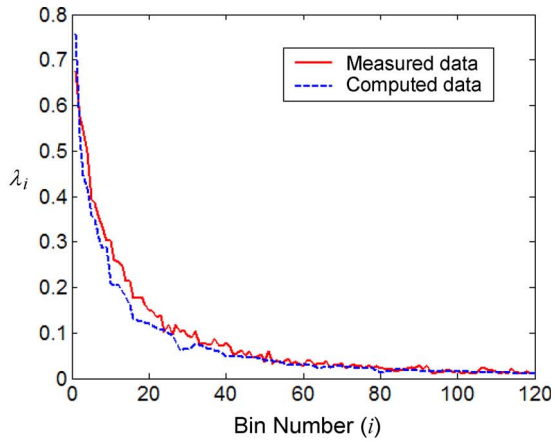

Fig. 9. Comparisons of the measured and computed results of (a) the path arrival rate λ_i and (b) the path occurrence probability P_i of the "Urban 1" site with 120 MHz bandwidth for $n = 4$.

TABLE III
VALUES OF $m_{e-\lambda}, \sigma_{e-\lambda}, m_{e-P}$, AND σ_{e-P} FOR $n = 4$

Measurement Sites	Bandwidth (F)	$m_{e\text{-}\lambda}$	$\sigma_{e\text{-}\lambda}$	$m_{e\text{-}P}$	$\sigma_{e\text{-}P}$
Urban 1	120 MHz	-0.1610	0.1134	-0.1423	0.1197
Urban 2	50 MHz	-0.1539	0.1187	-0.1501	0.1159
Suburban	50 MHz	-0.1711	0.1314	-0.1730	0.1288
Indoor LOS	2 GHz	-0.1643	0.1278	-0.1713	0.1256
Indoor NLOS	2 GHz	-0.1592	0.1309	-0.1625	0.1248

Table IV shows the average number of paths $\mathrm{NP}_{20\,\mathrm{dB}}$, which were calculated from the measured and computed results of P_i, respectively. It is found that the average number of paths is increased as the signal bandwidth is increased. In addition to the $m_{e-\lambda}$, $\sigma_{e-\lambda}$, m_{e-P}, and σ_{e-P} shown in Tables II and III, the good prediction accuracy of $\mathrm{NP}_{20\,\mathrm{dB}}$ shown in

TABLE IV
VALUES OF MEASURED AND COMPUTED $\mathrm{NP}_{20\,\mathrm{dB}}$

Measurement Sites	Bandwidth (F)	Measured $\mathrm{NP}_{20\mathrm{dB}}$	Computed $\mathrm{NP}_{20\mathrm{dB}}$ (computed from measured data @ 1/2×F)	Computed $\mathrm{NP}_{20\mathrm{dB}}$ (computed from measured data @ 1/4×F)
Urban 1	120 MHz	15.4	14.2	13.4
	60 MHz	11.8	11.2	---
	30 MHz	8.5	---	---
Urban 2	50 MHz	13.8	13.0	12.2
	25 MHz	10.6	10.1	---
	12.5 MHz	8.2	---	---
Suburban	50 MHz	12.8	12.0	11.3
	25 MHz	9.3	8.7	---
	12.5 MHz	6.9	---	---
Indoor LOS	2 GHz	25.3	22.8	19.6
	1 GHz	15.8	14.8	---
	0.5 GHz	11.8	---	---
Indoor NLOS	2 GHz	67.3	60.4	54.7
	1 GHz	38.3	35.4	---
	0.5 GHz	24.0	---	---

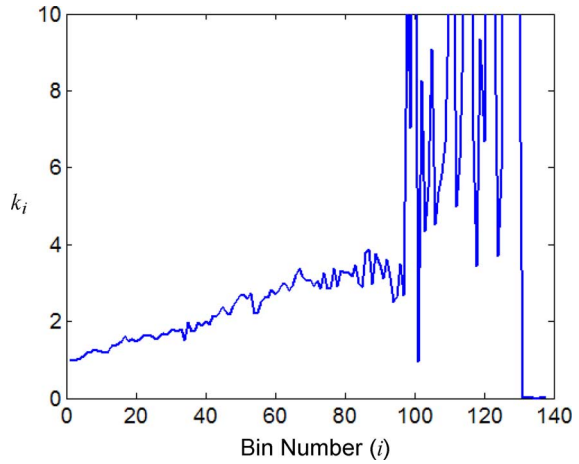

Fig. 10. Measured k_i of "Indoor NLOS" site with 1 GHz bandwidth.

Table IV also validates our proposed method. The mean value of relative errors of $\mathrm{NP}_{20\,\mathrm{dB}}$ are -0.0701 and -0.1551 for $n = 2$ and 4, respectively.

Fig. 10 illustrates the measured k_i of a 1-GHz-bandwidth signal at the "Indoor NLOS" site. It is found that k_i fluctuates at bins with a large bin number. It is noted that for clearly showing the small variation of k_i at bins with a small bin number, the values of k_i have been clipped at the far right of Fig. 10. From (16), it is easily understood that the fluctuation of k_i results from the very small values of λ_i, $N_{10,i}$, and $N_{11,i}$ for bins with long delays. However, these bins are insignificant to the value of channel parameters because of their very low powers. From Figs. 8 and 10, it is found that k_i varies slightly at bins with $\lambda_i \geq 0.1$ (bin number ≤ 80). Therefore, it is reasonable to use $\overline{K}$, which is defined as the mean value of k_i of the bins with $\lambda_i \geq 0.1$, as an index to quantify the observed multipath clustering.

$\overline{K}$ versus bandwidth curves at both the outdoor and indoor measurement sites are illustrated in Fig. 11(a) and (b), respectively. The figures show that $\overline{K}$ is increased when the signal bandwidth is increased, i.e., the wider bandwidth signal

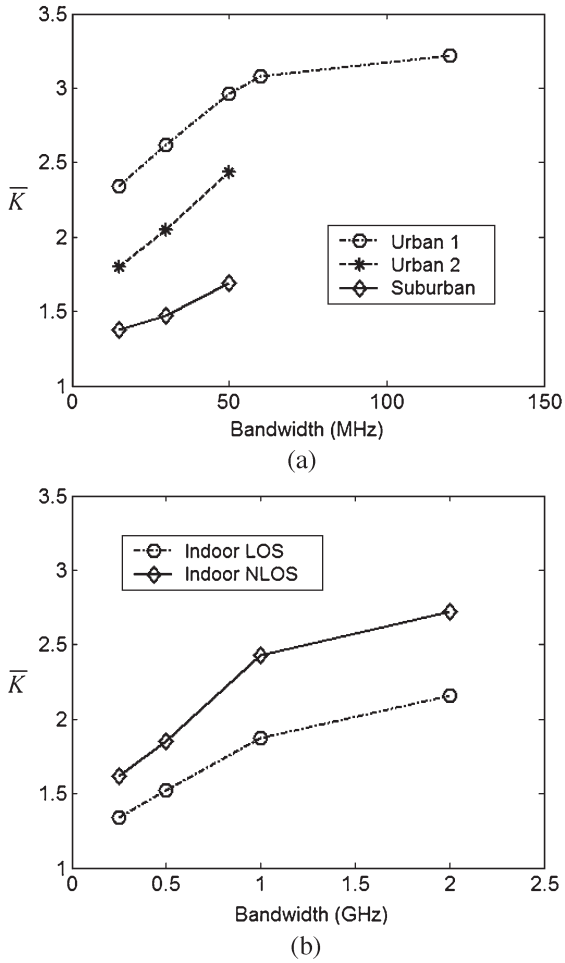

Fig. 11. $\overline{K}$ value of the measurement sites. (a) Outdoor environments. (b) Indoor environments.

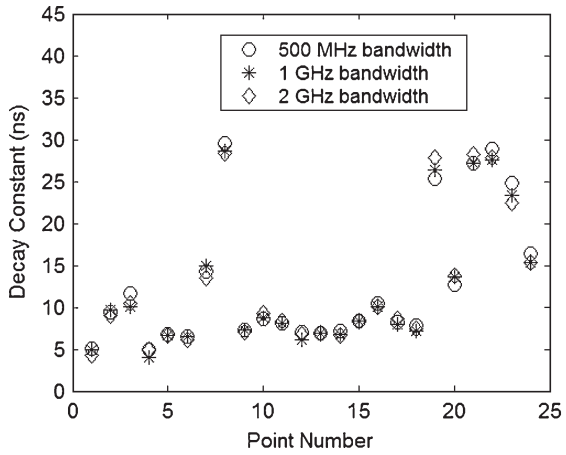

Fig. 12. Decay constant versus measured point number for signal bandwidths of 500 MHz, 1 GHz, and 2 GHz at "Indoor LOS" and "Indoor NLOS" sites.

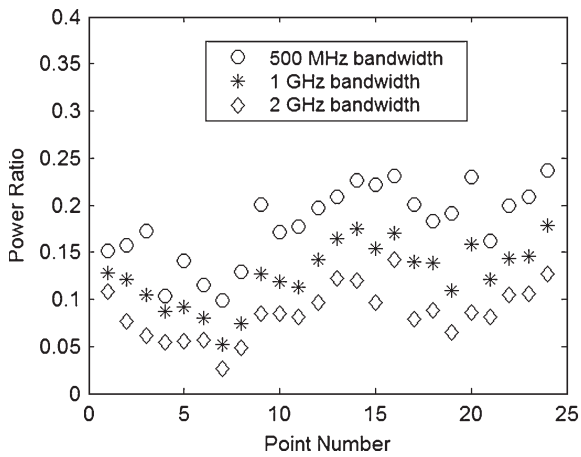

Fig. 13. Power ratio versus measured point number for signal bandwidths of 500 MHz, 1 GHz, and 2 GHz at "Indoor LOS" and "Indoor NLOS" sites.

yields stronger observable multipath clustering. It is because more paths may be resolved due to the finer time resolution of the signal, which increases the probability of clustering occurrence.

In Fig. 11(a), it is also found that the $\overline{K}$ value in an urban area is larger than that in the suburban area. It is simply because in urban areas, the scatterers (buildings) are denser and larger than those in the suburban areas, which leads to a larger chance of MPCs arriving in groups. For indoor environments, $\overline{K}$ in an LOS situation is smaller than that in the NLOS situation, as shown in Fig. 11(b). This is because the power of the direct path is much larger than that of the reflected and scattered paths under the LOS condition; most part of the grouping paths from scattering and multiple reflections cannot be detected.

Fig. 12 shows the decay constant versus measured point number for the "Indoor LOS" and "Indoor NLOS" sites with signal bandwidths of 500 MHz, 1 GHz, and 2 GHz. The comparison shows that the decay constant is independent of the signal bandwidth because there is only a little difference in the decay constant value among the three bandwidths at each measured point.

Fig. 13 shows the power ratio versus measured point number for the "Indoor LOS" and "Indoor NLOS" sites with signal bandwidths of 500 MHz, 1 GHz, and 2 GHz. It is found that the power ratio is decreased when the signal bandwidth is increased, which validates our analytical result, as shown in (10). Fig. 14 shows the measured and computed power ratio for a bandwidth of 1 GHz. Here, the computed results are based on the measured results of a 500-MHz-bandwdith signal and by using (12). The comparison shows that our proposed method yields a good prediction accuracy of the power ratio.

Fig. 15 shows the first bin's Rician factor versus measured point number for the "Indoor LOS" and "Indoor NLOS" sites with signal bandwidths of 500 MHz, 1 GHz, and 2 GHz. It is found that the Rician factor is increased when the signal bandwidth is increased for most of the measured points, which validates our analytical result, as shown in (11). Fig. 16 illustrates the measured and computed Rician factor for a bandwidth of 1 GHz. Here, the computed data for the 1-GHz-bandwidth signal is achieved from the measured data of a signal with 500 MHz bandwidth using (13). It is found that our proposed method yields a good prediction accuracy for the points with low Rician factors but leads to an overestimation for the points with large Rician factors. However, this kind of difference does not cause a significant impact on the small-scale fading statistical properties because the statistical properties of Rician fading are not very sensitive to large Rician factors [23].

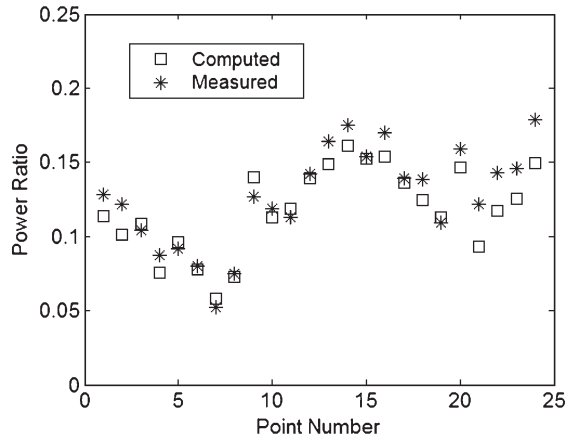

Fig. 14. Comparisons between the measured and computed results of the power ratio for all measured points at "Indoor LOS" and "Indoor NLOS" sites with 1 GHz bandwidth.

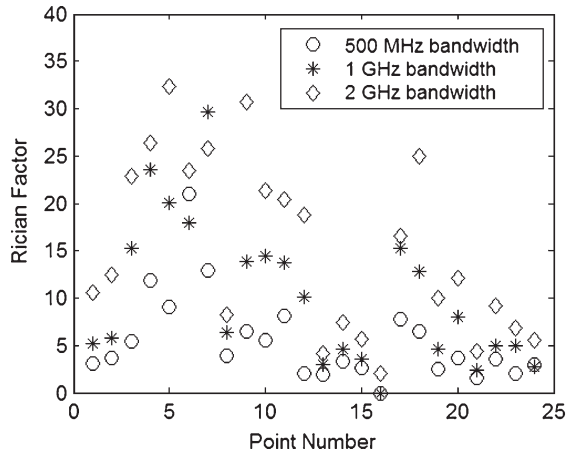

Fig. 15. Rician factor versus measured point number for signal bandwidths of 500 MHz, 1 GHz, and 2 GHz at "Indoor LOS" and "Indoor NLOS" sites.

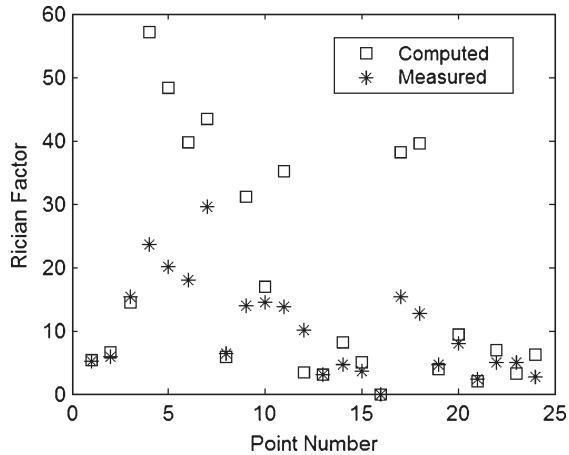

Fig. 16. Comparisons between the measured and computed results of the Rician factor for all measured points at "Indoor LOS" and "Indoor NLOS" sites with 1 GHz bandwidth.

VI. Conclusion

For a band-limited system, due to the limitation of the signal time resolution, the observation of the multipath clustering is a function not only of the propagation environment but also of the signal bandwidth. In this paper, with the help of the $\Delta - K$ model, the effect of signal bandwidth on observable multipath clustering is investigated by exploring the relationship between Δ, signal bin width, and $\overline{K}$—an index to quantify the multipath-clustering phenomenon. A formula is derived to show that the signal with a larger bandwidth yields finer time resolution and observes more MPCs, which may show stronger multipath clustering in iPDPs. To completely characterize the time dispersion characteristics of the channel, bandwidth dependences of multipath aPDP and amplitude fading are also formulated. Here, a model is applied to characterize the aPDP with two coefficients: the power ratio and decay constant. In addition, the amplitude fading is described by a Rician distribution function. It is found that 1) the power ratio is decreased when the signal bandwidth is increased, 2) the decay constant is independent of signal bandwidth, and 3) the Rician factor is increased as the signal bandwidth is increased. Our findings are validated by the measurement results of 1.95- and 2.44-GHz broadband signals in metropolitan and suburban areas and by the results of the 3–5-GHz UWB signals in indoors. In the future, we plan to investigate the dependency of the multipath clustering on the propagation environment, which needs extensive measurements.

References

[1] ITU-R PDNR, *Vision Framework and Overall Objectives of the Future Development of IMT-2000 and of Systems Beyond IMT-2000*, Jun. 2002.

[2] D. Porcino and W. Hirt, "Ultra-wideband radio technology: Potential and challenges ahead," *IEEE Commun. Mag.*, vol. 41, no. 7, pp. 66–74, Jul. 2003.

[3] FCC, "Revision of Part 15 of the Commission's Rules Regarding Ultra-Wideband Transmission Systems," *First Report and Order*. ET Docket 98-153, FCC 02-48, Apr. 2002.

[4] A. Saleh and R. Valenzuela, "A statistical model for indoor multipath propagation," *IEEE J. Sel. Areas Commun.*, vol. SAC-5, no. 2, pp. 128–137, Feb. 1987.

[5] H. Hashemi, "Impulse response modeling of indoor radio propagation channels," *IEEE J. Sel. Areas Commun.*, vol. 11, no. 7, pp. 967–978, Sep. 1993.

[6] H. Asplund, A. F. Molisch, M. Steinbauer, and N. B. Mehta, "Clustering of scatterers in mobile radio channels—Evaluation and modeling in the COST259 directional channel model," in *Proc. ICC*, Apr. 2002, vol. 2, pp. 901–905.

[7] K.-H. Li, M. A. Ingram, and A. V. Nguyen, "Impact of clustering in statistical indoor propagation models on link capacity," *IEEE Trans. Commun.*, vol. 50, no. 4, pp. 521–523, Apr. 2002.

[8] H. Suzuki, "A statistical model for urban radio propagation," *IEEE Trans. Commun.*, vol. COM-25, no. 7, pp. 673–680, Jul. 1977.

[9] R. J.-M. Cramer, R. A. Scholtz, and M. Z. Win, "Evaluation of an ultra-wide-band propagation channel," *IEEE Trans. Antennas Propag.*, vol. 50, no. 5, pp. 561–570, May 2002.

[10] Q. H. Spencer, B. D. Jeffs, M. A. Jensen, and A. L. Swindelhurst, "Modeling the statistical time and angle of arrival characteristics of an indoor multipath channel," *IEEE J. Sel. Areas Commun.*, vol. 18, no. 3, pp. 347–360, Mar. 2000.

[11] IEEE P802.15, *Channel Modeling Sub-Committee Report Final*, Feb. 2003. described in document IEEE P802.15-02/490r1-SG3a.

[12] R. Ganesh and K. Pahlavan, "Statistical modelling and computer simulation of indoor radio channel," *Proc. Inst. Electr. Eng., I*, vol. 138, no. 3, pp. 153–161, Jun. 1991.

[13] J. C. Sperandio and P. G. Flikkema, "Discrete-time Markov models for path delays in multipath channels," in *Proc. IEEE Int. Conf. Universal Pers. Commun.*, Sep. 1996, vol. 1, pp. 81–85.

[14] J. R. Foerster, "The effects of multipath interference on the performance of UWB systems in an indoor wireless channel," in *Proc. IEEE VTC—Spring*, May 2001, vol. 2, pp. 1176–1180.

[15] F. Zhu, Z. Wu, and C. R. Nassar, "Generalized fading channel model with application to UWB," in *Proc. IEEE Conf. Ultra Wideband Syst. and Technol.*, May 2002, pp. 13–17.
[16] G. L. Turin, F. D. Clapp, T. L. Johnston, S. B. Fine, and D. Lavry, "A statistical model of urban multipath propagation," *IEEE Trans. Veh. Technol.*, vol. VT-21, no. 1, pp. 1–9, Feb. 1972.
[17] G. L. Turin, W. S. Jewell, and T. L. Johnston, "Simulation of urban vehicle-monitoring systems," *IEEE Trans. Veh. Technol.*, vol. VT-21, no. 1, pp. 9–16, Feb. 1972.
[18] H. Hashemi, "Simulation of the urban radio propagation channel," *IEEE Trans. Veh. Technol.*, vol. VT-28, no. 3, pp. 213–225, Aug. 1979.
[19] D. Cassioli, M. Z. Win, and A. F. Molisch, "A statistical model for the UWB indoor channel," in *Proc. IEEE VTC—Spring*, May 2001, vol. 2, pp. 1159–1163.
[20] J. D. Parsons, *The Mobile Radio Propagation Channel*. London, U.K.: Pentech, 1992.
[21] R. S. Thomä, D. Hampicke, A. Richter, G. Sommerkom, A. Schneider, U. Trautwein, and W. Wirnitzer, "Identification of time-variant directional mobile radio channels," *IEEE Trans. Instrum. Meas.*, vol. 49, no. 2, pp. 357–364, Apr. 2000.
[22] R. Ganesh and K. Pahlavan, "On the modeling of fading multipath indoor radio channels," in *Proc. IEEE GLOBECOM*, Nov. 1989, vol. 3, pp. 1346–1350.
[23] N. Blaunstein and J. B. Anderson, *Multipath Phenomena in Cellular Networks*. London, U.K.: Artech House, 2002.

Wei-Ju Chang received the B.S. and M.S. degrees in communication engineering from the National Chiao Tung University, Hsinchu, Taiwan, R.O.C., in 1994 and 1996, respectively, where he is currently working toward the Ph.D. degree.

He has been with Chunghwa Telecom Laboratories, Taoyuan, Taiwan, since 1997 and is currently active in the fields of new air interface technologies for next-generation wireless communications.

Jenn-Hwan Tarng (S'85–M'89–SM'06) received the B.S. degree in power mechanical engineering from the National Tsin Hua University, Hsinchu, Taiwan, R.O.C., in 1981 and the M.S. and Ph.D. degrees in electrical engineering from Pennsylvania State University, University Park, in 1988 and 1989, respectively.

He is a Professor in the Department of Communication Engineering, National Chiao Tung University, Hsinchu. His professional interests include radio propagation modeling and measurement, radio allocation, radio network planning, smart antennas systems, and EMC.